Catastrophic locking of the $m/n = 1/1$ mode in sawtoothing tokamak plasmas

C. E. Myers,[1,*] N. M. Ferraro,[1] J.-K. Park,[1] S. P. Gerhardt,[1] J. E. Menard,[1] R. E. Bell,[1] B. P. LeBlanc,[1] M. Podestà,[1] and S. A. Sabbagh[2]

[1] *Princeton Plasma Physics Laboratory, Princeton, NJ 08543, USA*
[2] *Columbia University, New York, New York 10027, USA*

(Dated: October 3, 2017)

Non-axisymmetric 'error' fields can severely constrain the performance of tokamaks. Sufficiently large error fields can open magnetic islands at mode-rational surfaces and lock the rotation of the plasma, often resulting in a disruption. The conventional understanding is that the $m/n = 2/1$ mode is the critical mode that must be avoided to prevent disruptions, even in the sawtoothing regime where the plasma core is inherently unstable. Here we show for the first time, however, that a different mode can lock and disrupt the plasma: the 1/1 core mode. In the National Spherical Torus Experiment Upgrade (NSTX-U), sawtoothing plasmas exhibit two key features of 1/1 locking: (1) they are highly sensitive to 1/1 error fields; and (2) a large $n = 1$ magnetic island forms at the $q = m/n = 1$ mode-rational surface at the onset of locking. Given that ITER, the flagship next-generation tokamak, intends to operate in the sawtoothing regime, the NSTX-U results indicate that every effort should be made to minimize intrinsic 1/1 error fields during ITER assembly.

The outsized impact of small non-axisymmetric 'error' magnetic fields on tokamak stability has long been recognized [1–8]. The most consequential error fields are those that resonate with mode-rational magnetic surfaces, which are defined by a rational value of the safety factor, $q = m/n$, where m and n are the poloidal and toroidal mode numbers. If a resonant error field is large enough, it can cause the plasma to suddenly transition to a low-rotation 'locked' state with a magnetic island at the mode-rational surface [9, 10]. Such mode locking events often cause the plasma to disrupt [11].

The most virulent error fields are those with a toroidal mode number of $n = 1$ and small values of the poloidal mode number, m. In particular, $m/n = 2/1$ error fields have been empirically identified as the most important perturbations that must be suppressed to avoid locking [3–8, 12–15]. Fortunately, great progress has been made toward understanding the plasma response to 2/1 error fields [16–19]. This has led to expanded operating regimes in both conventional and high-aspect-ratio devices [2, 12, 13, 20, 21]. The importance of low m values begs the question, however, as to why 1/1 error fields are not even more virulent than 2/1 error fields in plasmas with $q_{\min} \leq 1$ (i.e., plasmas with a 1/1 mode-rational surface). The answer is that such plasmas are inherently unstable to a 1/1 internal kink or 'sawtooth' mode [22] that has previously been observed to be insensitive to 1/1 perturbations [4]. As such, the potential for catastrophic 1/1 locking has historically been ignored.

In this paper, we report the first observation of 1/1 mode locking in a tokamak. These results, which were obtained in the National Spherical Torus Experiment Upgrade (NSTX-U) [23], indicate that 1/1 locking can occur in sawtoothing plasmas whose error field response is dominated by 1/1 rather than 2/1 resonant fields. These findings present a challenge both for standard error field correction techniques and for state-of-the-art plasma response modeling. They therefore motivate renewed efforts to understand, mitigate, and correct 1/1 intrinsic error fields in future tokamaks such as ITER that will operate in the sawtoothing regime [24].

The vacuum error fields in NSTX-U are derived from multiple sources. The largest intrinsic (unintended) error fields are generated on the high field side by an $\mathcal{O}(10^{-3})$ shift and tilt of the center rod of the toroidal field (TF) coil (see Fig. 1a) [25]. The 1/1 and 2/1 components of the resulting TF-generated error fields are shown in Fig. 1c. Vacuum error fields can also be deliberately applied to the plasma using a set of six non-axisymmetric error field correction (EFC) coils located at the outboard midplane (see Fig. 1b). Here, these coils are configured to apply $n = 1$ fields at any desired toroidal phase (see Fig. 1c).

The first indication that NSTX-U discharges are susceptible to 1/1 mode locking is that the plasma response to the vacuum error fields changes drastically when the $q = 1$ mode-rational surface enters the plasma. This effect is demonstrated in Fig. 2 where three 1 MW beam-heated L-mode plasma discharges with different EFC settings are compared. First, in the 'best ramp-up' case, the EFC settings are chosen to maximize performance in the ramp-up phase of discharge (i.e., with no $q = 1$ surface). In the 'best flattop' case, on the other hand, the EFC settings are chosen to maximize performance in the flattop phase (i.e., with a $q = 1$ surface). The 'no correction' case serves as a reference. As shown in Fig. 2b, the 'best ramp-up' and 'best flattop' EFC settings, which were determined from dedicated EFC optimization experiments, have comparable EFC amplitudes ($I_{\mathrm{EFC}} \simeq 600\,\mathrm{A}$) but very different EFC phases ($\phi_{\mathrm{EFC}} \simeq 209°$ versus 76°).

The plasma response to the applied EFC fields is assessed using high-cadence measurements of impurity carbon ion rotation in the core of the plasma (see Fig. 2c) [26]. The faster the rotation, the smaller the magnetohydrodynamic drag and the smaller the plasma

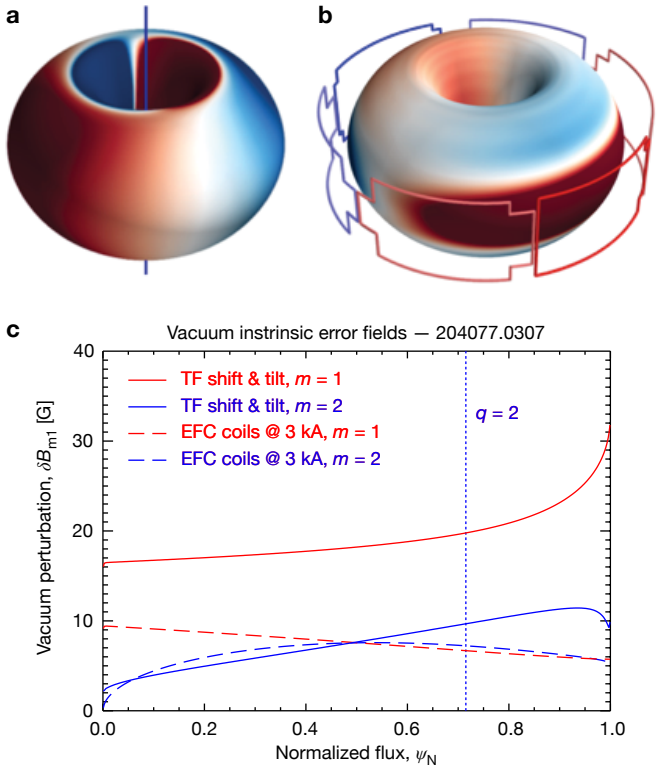

FIG. 1. Calculations of the non-axisymmetric vacuum magnetic fields created **a**, by a misalignment of the toroidal field (TF) center rod; and **b**, by the six error field correction (EFC) coils at the outboard midplane. The colors in the coils represent positive or negative current, while the colors on the sample plasma surface represent positive or negative normal perturbed magnetic field. **c**, The $m = 1, 2$ components of the $n = 1$ vacuum field perturbations, δB_{m1}, generated by the shift and tilt of the TF center rod (solid lines) and by the EFC coils (dashed lines) when operated near full current ($I_{\mathrm{EFC}} = 3\,\mathrm{kA}$ or $6\,\mathrm{kA}$-turns). The normalized flux, ψ_{N}, that defines the abscissa is a poloidal flux function that runs from zero at the center of the plasma to unity at the edge.

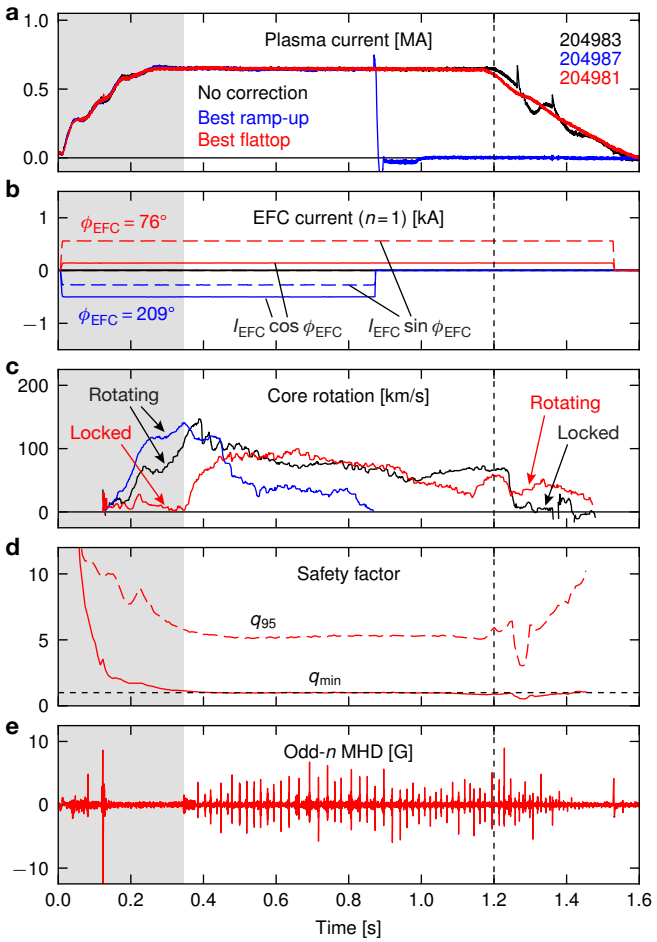

FIG. 2. **a**, Plasma current waveforms from three 1 MW beam-heated L-mode discharges with different applied EFC currents. The toroidal field on axis is $B_{\mathrm{T}} \simeq 0.63\,\mathrm{T}$, and the flattop plasma current is $I_{\mathrm{p}} \simeq 650\,\mathrm{kA}$. **b**, Sine and cosine components of the $n = 1$ EFC coil currents. The 'best ramp-up' and 'best flattop' cases have similar applied EFC amplitudes ($I_{\mathrm{EFC}} \sim 600\,\mathrm{A}$) but different EFC phases ($\phi_{\mathrm{EFC}} = 209°$ versus 76°). **c**, Evolution of the toroidal rotation of carbon ion impurities in the core. **d**, Evolution of the safety factor both in the core, q_{min}, and near the edge, q_{95}, in discharge 204981 as determined from magnetic equilibrium reconstructions of the plasma. **e**, Odd-n low-frequency MHD activity in discharge 204981 as determined by differencing two toroidally opposed Mirnov sensors inside the NSTX-U vessel. The periodic bursts of MHD activity after $t \simeq 0.350\,\mathrm{s}$ are generated by sawtooth crashes in the $q_{\mathrm{min}} \leq 1$ core.

response. First, during the ramp-up phase ($t < 0.350\,\mathrm{s}$, shaded in gray), three different rotation rates are observed: the 'best ramp-up' case rotates the fastest, followed by the reference case. The 'best flattop' case, on the other hand, is locked entirely. After $t = 0.350\,\mathrm{s}$, however, the situation quickly reverses: The 'best flattop' case spins up, while the 'best ramp-up' case spins down and eventually locks and disrupts. The key change at $t = 0.350\,\mathrm{s}$ is that the $q = 1$ surface enters the plasma. This is indicated both by the q_{min} trace in Fig. 2d, which is extracted from magnetic equilibrium reconstructions of the plasma, and by the onset of the 1/1 sawtooth mode in the core of the plasma (see the MHD activity in Fig. 2e).

The rapid changes in the plasma response when q_{min} reaches unity are a key indicator that the sawtoothing core of the plasma interacts strongly with 1/1 resonant error fields. Further evidence can be found in the ramp-down phase of the discharge, which begins at $t = 1.2\,\mathrm{s}$. During this phase, the reference case suffers multiple mode locking events, which are visible both in the plasma current trace in Fig. 2a and in the core rotation trace in Fig. 2c. The 'best flattop' case, on the other hand, continues to rotate as the current smoothly ramps to zero. Figure 2e shows that the sawtooth events also continue throughout this ramp-down phase. As such, we conclude that the interaction of the sawtoothing core with 1/1 resonant fields dominates the plasma response through both the flattop and the ramp-down phases of these discharges.

To understand the nature of mode locking in the sawtoothing plasma scenario introduced in Fig. 2, we now

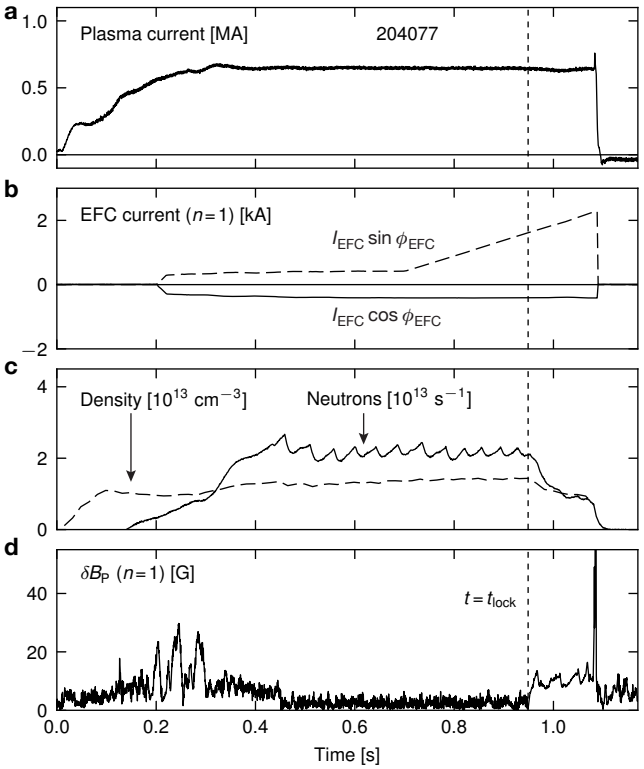

FIG. 3. **a**, Plasma current waveform for a 1 MW beam-heated L-mode discharge with deliberately induced mode locking. **b**, Sine and cosine components of the $n = 1$ EFC coil currents. Starting at $t = 0.7$ s, the sine component is linearly ramped upward from its initial value. **c**, Line-averaged plasma density and neutron rate. The sawtooth events are clearly visible in the neutron rate during the flattop. **d**, $n = 1$ poloidal magnetic field signal, δB_P. Spurious signals during the early phase ($t < 0.5$ s) can be ignored. A clear $n = 1$ locked mode is detected at $t_{lock} \simeq 0.949$ s as the ramping EFC fields penetrate into the core of the plasma.

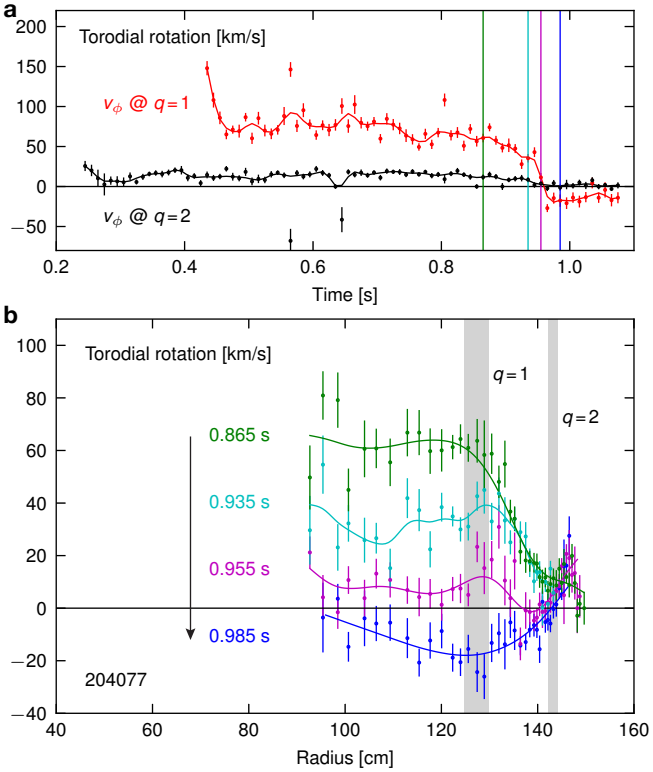

FIG. 4. **a**, Temporal evolution of the toroidal rotation, v_ϕ, at the $q = 1$ and $q = 2$ surfaces. The rational surface locations are extracted from magnetic equilibrium reconstructions of the plasma and then mapped to spatial profiles of toroidal rotation as determined from carbon impurity ion charge exchange recombination spectroscopy (CHERS) . **b**, Selected spatial profiles of toroidal rotation during locking. See the text for further details.

examine a deliberately induced mode locking event. As shown in Fig. 3, mode locking is induced by ramping the sine component of the EFC coil currents linearly upward from its initial value starting at $t = 0.7$ s (see Fig. 3b). During the EFC coil current ramp, the discharge continues its standard sawtoothing flattop evolution as indicated by the neutron rate signal in Fig. 3c. At $t \simeq 0.949$ s, however, the EFC fields become large enough to penetrate into the core of the plasma and generate an $n = 1$ locked mode (see Fig. 3d). This mode is born locked with no rotating precursor, and the sawtooth events cease immediately at the onset of locking. While many similar discharges in NSTX-U terminate shortly after locking, this example does not disrupt immediately, thereby providing an opportunity to investigate the plasma structure before, during, and after the mode locking event.

Figure 4 plots the temporal and spatial profiles of toroidal rotation during the deliberately induced mode locking event. First, Fig. 4a shows the temporal evolution of the toroidal rotation at the $q = 1$ and $q = 2$ surfaces. The $q = 2$ surface is locked from the outset, likely in response to the TF-generated 2/1 error fields described in Fig. 1. It proceeds to rotate very slowly ($v_\phi \sim 15$ km/s) throughout the flattop. The $q = 1$ surface, on the other hand, rotates much more rapidly. It initially enters the plasma at $t \sim 0.450$ s with a velocity of ~ 150 km/s, but it quickly spins down as it interacts with the TF-generated 1/1 error fields described in Fig. 1. Unlike the $q = 2$ surface, the $q = 1$ surface continues to rotate briskly ($v_\phi \sim 60$–80 km/s) for much of the flattop. While some braking is observed during the EFC coil current ramp starting at $t \simeq 0.7$ s, the core rotation does not collapse until the onset of mode locking at $t_{lock} \simeq 0.949$ s.

The details of the rotation collapse during the mode locking event are shown in Fig. 4b. Here we see that the rotation profile across the core of plasma is relatively flat. Between the $q = 1$ and $q = 2$ surfaces, on the other hand, a steep rotation gradient separates the rotating core from the locked $q = 2$ surface. During the mode locking event, the rotation across the core collapses. Because the $q = 2$ surface is already locked, however, there is minimal change in its rotation. This lack of change at $q = 2$ is a preliminary indication that the 2/1 mode is not the

primary cause of the mode locking event.

To unambiguously identify the structure of the mode that locks the plasma, we now turn to spatial profiles of the electron temperature, T_e, obtained from Thomson scattering. Figure 5 plots T_e profiles from before, during, and after the mode locking event. Prior to locking, the plasma exhibits periodic sawtoothing behavior where the T_e profile peaks in the core prior to each sawtooth crash and flattens shortly thereafter. The spatial extent of these sawtooth oscillations confirms the location of the $q = 1$ surface from magnetic equilibrium reconstructions.

At the onset of locking, the T_e profile deviates sharply from its sawtoothing behavior in a way that reveals the structure of the mode that causes the plasma to lock. More specifically, the T_e profile highlighted in red, which is acquired at the onset of locking at $t = 0.948$ s, shows that a large island forms at the location of the $q = 1$ surface on the inboard side of the T_e profile. The island is identified as a distinct flattening of the T_e profile that spans several Thomson diagnostic channels. In concert with the magnetic measurements of an $n = 1$ locked mode from Fig. 3d, this observation of island formation at the $q = m/n = 1$ surface confirms that the mode that locks the plasma is, in fact, an $m/n = 1/1$ mode.

An equally important conclusion from the T_e profiles in Fig. 5 is that no meaningful change is observed at the $q = 2$ surface at the onset of locking. More specifically, the red T_e profile remains within the narrow envelope at the $q = 2$ surface that is established during the sawtoothing phase of the discharge. As such, no large 2/1 island is observed to modify the T_e profile, which supports the conclusion that this event is driven instead by the locking of a 1/1 mode. Finally, once mode locking is complete, the T_e profile settles into a new equilibrium for the remainder of the discharge. This post-locking T_e profile is entirely flat across the core of the plasma.

The 1/1 mode locking results presented here have profound implications for the stability of tokamaks that seek to operate in the sawtoothing regime, including ITER [24]. First, the NSTX-U results indicate that ITER should make every effort to minimize intrinsic 1/1 error fields in order to avoid 1/1 mode locking in its sawtoothing scenarios. Second, the NSTX-U results raise challenging questions as to what causes sawtoothing plasmas in NSTX-U to be so strongly impacted by 1/1 resonant error fields. One possibility is that the large TF-generated high-field-side error fields interact with the plasma in a way that substantially increases its sensitivity to 1/1 perturbations. This possibility motivates dedicated high-field-side error field experiments in a tokamak such as COMPASS that can apply external high-field-side perturbations [27].

The NSTX-U results also highlight the need for more accurate modeling of the plasma response to 1/1 resonant fields in the sawtoothing regime. Unfortunately, state-of-the-art techniques such as perturbed equilibrium modeling are unable to treat sawtoothing plasmas because such plasmas reside in a state of continuous instability rather than quiescent equilibrium. As such, more challenging and expensive nonlinear magnetohydrodynamic calculations are required. Regardless, the potential for 1/1 mode locking to limit the stability and performance of sawtoothing plasmas provides renewed motivation for such modeling efforts. Ultimately, the understanding gained from improved modeling of the 1/1 plasma response will inform the alignment tolerances placed on the toroidal field coils and other sources of 1/1 error fields in ITER.

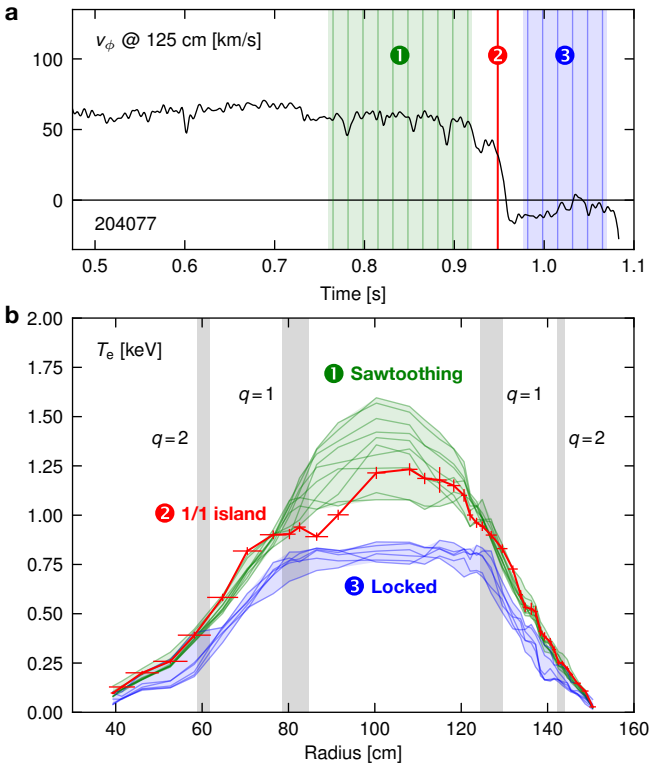

FIG. 5. Evolution of the electron temperature profile, T_e, as measured by Thomson scattering. **a**, Vertical lines mark the times at which the various T_e profiles are acquired. The toroidal rotation, v_ϕ, at $R = 125$ cm is shown for reference. **b**, The various T_e profiles are color-coded based on whether they occur before (1/green), during (2/red), or after (3/blue) the mode locking event. The locations of the inboard and outboard $q = 1$ and $q = 2$ mode-rational surfaces from magnetic equilibrium reconstructions are shown in gray. The clear co-location of the sawtooth inversion radius with the $q = 1$ surface validates the reconstruction results. A large 1/1 island is visible on the inboard side of the T_e profile at the time of locking. See the text for further details.

The authors thank D. J. Battaglia, M. D. Boyer, W. Guttenfelder, S. M. Kaye, D. Mueller, and the NSTX-U team for their support of these experiments. This research is supported by U.S. Department of Energy contract number DE-AC02-09CH11466. The digital data for this paper can be found at `http://dataspace.princeton.edu/jspui/handle/88435/dsp01j6731612k`.

* cmyers@pppl.gov

[1] J. A. Snipes, D. J. Campbell, P. S. Haynes, T. C. Hender, M. Hugon, P. J. Lomas, N. J. L. Cardozo, M. F. F. Nave, and F. C. Schüller, Nuclear Fusion **28**, 1085 (1988).

[2] J. T. Scoville, R. J. La Haye, A. G. Kellman, T. H. Osborne, R. D. Stambaugh, E. J. Strait, and T. S. Taylor, Nucl. Fusion **31**, 875 (1991).

[3] A. W. Morris, P. G. Carolan, R. Fitzpatrick, T. C. Hender, and T. N. Todd, Phys. Fluids B **4**, 413 (1992).

[4] T. C. Hender, R. Fitzpatrick, A. W. Morris, P. G. Carolan, R. D. Durst, T. Edlington, J. Ferreira, S. J. Fielding, P. S. Haynes, J. Hugill, I. J. Jenkins, R. J. La Haye, B. J. Parham, D. C. Robinson, T. N. Todd, M. Valovic, and G. Vayakis, Nucl. Fusion **32**, 2091 (1992).

[5] R. J. La Haye, R. Fitzpatrick, T. C. Hender, A. W. Morris, J. T. Scoville, and T. N. Todd, Phys. Fluids B **4**, 2098 (1992).

[6] R. J. La Haye, A. W. Hyatt, and J. T. Scoville, Nucl. Fusion **32**, 2119 (1992).

[7] G. Fishpool and P. Haynes, Nucl. Fusion **34**, 109 (1994).

[8] R. J. Buttery, M. De' Benedetti, D. A. Gates, Y. Gribov, T. C. Hender, R. J. La Haye, P. Leahy, J. A. Leuer, A. W. Morris, A. Santagiustina, J. T. Scoville, B. J. D. Tubbing, JET Team, COMPASS-D Research Team, and DIII-D Team, Nucl. Fusion **39**, 1827 (1999).

[9] R. Fitzpatrick and T. C. Hender, Phys. Fluids B **3**, 644 (1991).

[10] R. Fitzpatrick, Nucl. Fusion **33**, 1049 (1993).

[11] P. C. de Vries, M. F. Johnson, B. Alper, P. Buratti, T. C. Hender, H. R. Koslowski, V. Riccardo, and JET-EFDA Contributors, Nucl. Fusion **51**, 053018 (2011).

[12] S. M. Wolfe, I. H. Hutchinson, R. S. Granetz, J. Rice, A. Hubbard, A. Lynn, P. Phillips, T. C. Hender, D. F. Howell, R. J. La Haye, and J. T. Scoville, Phys. Plasmas **12**, 056110 (2005).

[13] D. F. Howell, T. C. Hender, and G. Cunningham, Nucl. Fusion **47**, 1336 (2007).

[14] J. E. Menard, R. E. Bell, D. A. Gates, S. P. Gerhardt, J.-K. Park, S. A. Sabbagh, J. W. Berkery, A. Egan, J. Kallman, S. M. Kaye, B. LeBlanc, Y. Q. Liu, A. Sontag, D. Swanson, H. Yuh, W. Zhu, and the NSTX Research Team, Nucl. Fusion **50**, 045008 (2010).

[15] A. Kirk, Y. Liu, R. Martin, G. Cunningham, D. Howell, and the MAST Team, Plasma Phys. Control. Fusion **56**, 104003 (2014).

[16] A. H. Boozer, Phys. Rev. Lett. **86**, 5059 (2001).

[17] J.-K. Park, A. H. Boozer, and A. H. Glasser, Phys. Plasmas **14**, 052110 (2007).

[18] J.-K. Park, M. J. Schaffer, J. E. Menard, and A. H. Boozer, Phys. Rev. Lett. **99**, 195003 (2007).

[19] Y. Liu, A. Kirk, and E. Nardon, Phys. Plasmas **17**, 122502 (2010).

[20] R. J. Buttery, M. De' Benedetti, T. C. Hender, and B. J. D. Tubbing, Nucl. Fusion **40**, 807 (2000).

[21] J. E. Menard, M. G. Bell, R. E. Bell, E. D. Fredrickson, D. A. Gates, S. M. Kaye, B. P. LeBlanc, R. Maingi, D. Mueller, S. A. Sabbagh, D. Stutman, C. E. Bush, D. W. Johnson, R. Kaita, H. W. Kugel, R. J. Maqueda, F. Paoletti, S. F. Paul, M. Ono, Y.-K. M. Peng, C. H. Skinner, E. J. Synakowski, and the NSTX Research Team, Nucl. Fusion **43**, 330 (2003).

[22] S. von Goeler, W. Stodiek, and N. Sauthoff, Phys. Rev. Lett. **33**, 1201 (1974).

[23] J. E. Menard, J. P. Allain, D. J. Battaglia, F. Bedoya, R. E. Bell, E. Belova, J. W. Berkery, M. D. Boyer, N. Crocker, A. Diallo, F. Ebrahimi, N. Ferraro, E. Fredrickson, H. Frerichs, S. Gerhardt, N. Gorelenkov, W. Guttenfelder, W. Heidbrink, R. Kaita, S. M. Kaye, D. M. Kriete, S. Kubota, B. P. LeBlanc, D. Liu, R. Lunsford, D. Mueller, C. E. Myers, M. Ono, J.-K. Park, M. Podesta, R. Raman, M. Reinke, Y. Ren, S. A. Sabbagh, O. Schmitz, F. Scotti, Y. Sechrest, C. H. Skinner, D. R. Smith, V. Soukhanovskii, T. Stoltzfus-Dueck, H. Yuh, Z. Wang, I. Waters, J.-W. Ahn, R. Andre, R. Barchfeld, P. Beiersdorfer, N. Bertelli, A. Bhattacharjee, D. Brennan, R. Buttery, A. Capece, G. Canal, J. Canik, C. S. Chang, D. Darrow, L. Delgado-Aparicio, C. Domier, S. Ethier, T. Evans, J. Ferron, M. Finkenthal, R. Fonck, K. Gan, D. Gates, I. Goumiri, T. Gray, J. Hosea, D. Humphreys, T. Jarboe, S. Jardin, M. A. Jaworski, B. Koel, E. Kolemen, S. Ku, R. J. L. Haye, F. Levinton, N. Luhmann, R. Maingi, R. Maqueda, G. McKee, E. Meier, J. Myra, R. Perkins, F. Poli, T. Rhodes, J. Riquezes, C. Rowley, D. Russell, E. Schuster, B. Stratton, D. Stutman, G. Taylor, K. Tritz, W. Wang, B. Wirth, and S. J. Zweben, Nucl. Fusion **57**, 102006 (2017).

[24] T. C. Hender, J. C. Wesley, J. Bialek, A. Bondeson, A. H. Boozer, R. J. Buttery, A. Garofalo, T. P. Goodman, R. S. Granetz, Y. Gribov, O. Gruber, M. Gryaznevich, G. Giruzzi, S. Günter, N. Hayashi, P. Helander, C. C. Hegna, D. F. Howell, D. A. Humphreys, G. T. A. Huysmans, A. W. Hyatt, A. Isayama, S. C. Jardin, Y. Kawano, A. Kellman, C. Kessel, H. R. Koslowski, R. J. La Haye, E. Lazzaro, Y. Q. Liu, V. Lukash, J. Manickam, S. Medvedev, V. Mertens, S. V. Mirnov, Y. Nakamura, G. Navratil, M. Okabayashi, T. Ozeki, R. Paccagnella, G. Pautasso, F. Porcelli, V. D. Pustovitov, V. Riccardo, M. Sato, O. Sauter, M. J. Schaffer, M. Shimada, P. Sonato, E. J. Strait, M. Sugihara, M. Takechi, A. D. Turnbull, E. Westerhof, D. G. Whyte, R. Yoshino, H. Zohm, and the ITPA MHD, Disruption and Magnetic Control Topical Group, Nucl. Fusion **47**, S128 (2007).

[25] C. E. Myers, N. M. Ferraro, S. P. Gerhardt, J. E. Menard, J.-K. Park, D. J. Battaglia, R. E. Bell, M. D. Boyer, B. P. LeBlanc, D. Mueller, M. Podestà, and S. A. Sabbagh, (2017), In preparation for Nucl. Fusion.

[26] M. Podestà and R. E. Bell, Plasma Phys. Control. Fusion **58**, 125016 (2016).

[27] R. Pánek, J. Adámek, M. Aftanas, P. Bílková, P. Böhm, F. Brochard, P. Cahyna, J. Cavalier, R. Dejarnac, M. Dimitrova, O. Grover, J. Harrison, P. Háček, J. Havlíček, A. Havránek, J. Horáček, M. Hron, M. Imríšek, F. Janky, A. Kirk, M. Komm, K. Kovařík, J. Krbec, L. Kripner, T. Markovič, K. Mitošinková, J. Mlynář, D. Naydenkova, M. Peterka, J. Seidl, J. Stöckel, E. Štefániková, M. Tomeš, J. Urban, P. Vondráček, M. Varavin, J. Varju, V. Weinzettl, J. Zajac, and the COMPASS team, Plasma Phys. Control. Fusion **58**, 014015 (2016).